Raman spectroscopy of blood and urine liquid biopsies for ovarian cancer diagnosis: identification of chemotherapy effects

Panagiotis Giamougiannis[1,2], Raissa V. O. Silva[3], Daniel L. D. Freitas[3], Kássio M. G. Lima[3], Antonios Anagnostopoulos[1], Georgios Angelopoulos[1], Raj Naik[1], Nicholas J. Wood[1], Pierre L. Martin-Hirsch[1], Francis L. Martin[4]*

1. Department of Obstetrics and Gynaecology, Lancashire Teaching Hospitals NHS Foundation Trust, Preston PR2 9HT, UK

2. School of Pharmacy and Biomedical Sciences, University of Central Lancashire, Preston PR1 2HE, UK

3. Institute of Chemistry, Biological Chemistry and Chemometrics, Federal University of Rio Grande do Norte, Natal, Brazil

4. Biocel Ltd, Hull HU10 7TS, UK

***Corresponding author:** Professor Francis L. Martin, Biocel Ltd, Hull HU10 7TS, UK.
*Email: flm13@biocel.uk

AUTHOR CONTRIBUTIONS

P.G. performed the sample collection, spectral data acquisition and analysis, and wrote the first manuscript draft. R.V.O.S., D.L.D.F. and K.M.G.L. performed the multivariate data analysis and aided writing the manuscript. A.A., G.A., R.N. and N.J.W. contributed in sample collection and edited the manuscript. F.L.M. conceived the study design. P.L.M. and F.L.M. supervised the project as principal investigators and finalised the manuscript.

Abstract

Blood plasma and serum Raman spectroscopy for ovarian cancer diagnosis has been applied in pilot studies, with promising results. Herein, a comparative analysis of these biofluids, with a novel assessment of urine, was conducted by Raman spectroscopy application in a large patient cohort. Spectra were obtained through samples measurements from 116 ovarian cancer patients and 307 controls. Principal component analysis identified significant spectral differences between cancers without previous treatment (n=71) and following neo-adjuvant chemotherapy - NACT (n=45). Application of five classification algorithms achieved up to 73% sensitivity for plasma, high specificities and accuracies for both blood biofluids, and lower performance for urine. A drop in sensitivities for the NACT group in plasma and serum, with an opposite trend in urine, suggest that Raman spectroscopy could identify chemotherapy-related changes. This study confirms that biofluids' Raman spectroscopy can contribute in ovarian cancer's diagnostic work-up and demonstrates its potential in monitoring treatment response.

Introduction

Despite numerous attempts to identify effective screening and diagnostic modalities, early detection of ovarian cancer remains elusive. Although it is globally the 8th most common cancer-related cause of death in women, it consists the most lethal gynaecological malignancy. This is due to its vague symptoms, leading to the majority of cases (over 70%) being diagnosed when the disease is already at widely disseminated metastatic stage [1-3]. Its most frequent type is by far the epithelial one (90% of ovarian malignancies) including several histological sub-types (such as serous, endometrioid, mucinous, clear cell carcinomas and carcinosarcomas), with high-grade serous cancers representing up to 80% of all cases. Less common types include germ cell and stromal tumours [3, 4]. Surgery and chemotherapy are the current mainstays of treatment, with platins (cisplatin or carboplatin) and taxanes (paclitaxel) being the most commonly used chemotherapy agents. When complete cytoreduction with upfront operating is not considered feasible, regimes known as neo-adjuvant chemotherapy (NACT) are administered before and after interval debulking surgery (IDS) [4, 5].

No ‘’gold standard’’ test exists for screening or diagnosis of ovarian cancer. Serum biomarkers (such as the cancer antigen CA125 and the human epididymis protein HE4), either alone or incorporated in predictive models using pelvic ultrasonography, have failed to produce significant reduction in mortality rates [6-9]. The diagnostic accuracy of CA125, the most commonly used tumour marker, is limited as many benign conditions (*e.g.* ovarian cysts, fibroids, endometriosis, adenomyosis) can also raise its levels [10, 11]. With regards to radiology modalities, more advanced imaging techniques than ultrasound (such as computed tomography, magnetic resonance imaging) are expensive, time-consuming and often associated with increased patient discomfort.

These limitations fuel the need for new methodologies in ovarian cancer detection. A potential candidate is vibrational spectroscopy, a bio-analytical tool that has shown capacity in identifying pathological conditions [12]. Raman is a powerful vibrational spectroscopic technique for biological materials

analysis, with previous applications including human tissues and biofluids [13]. It detects changes in molecular polarisation caused by a monochromatic laser source, which result in inelastic photon scattering (known as Raman shift), and produce a spectrum with peaks corresponding to wavelengths at which the scattering occurred [14]. Easily collectable biofluids, such as blood and urine, are ideal as liquid biopsies for investigations towards cancer diagnosis, as they are readily available and require minimal sample preparation [15]. Raman spectroscopy applications for these two biofluids have involved breast [16, 17], prostate [18, 19], bladder [20, 21], gastrointestinal [22-27] and cervical [28, 29] carcinomas. Performance of blood-derived biofluids (but not urine) has also been explored in ovarian cancer by small pilot studies [30-32], with promising results.

Herein, the potential of Raman spectroscopy for ovarian cancer diagnosis was further investigated, through analyses in blood and urine samples from a large patient cohort. The multivariate nature of biospectroscopy data requires application of chemometric techniques for extraction of good quality results that can be clinically translated [14]. In this study, a variety of chemometric methods were used for segregation of ovarian malignancies from a wide range of benign gynaecological conditions, including linear discriminant classifiers, support vector machines and genetic algorithms. Additionally, the effect of chemotherapy on spectral signatures was explored in those ovarian cancer patients who had received NACT.

Materials and Methods

Patients and samples

Between April 2018 and November 2019 four hundred and twenty three (n=423) consecutive patients were recruited (n=116 with ovarian cancer, n=307 with benign gynaecological conditions - controls). The majority of ovarian cancer patients had not received chemotherapy (n=71) whereas the rest had received

NACT (*n*=45). For the latter group, the median number of NACT cycles was 4 with a median interval of 3 weeks between cycles; 41 patients received a combination of carboplatin and paclitaxel and 4 patients single agent carboplatin. Samples were collected after informed consent upon patients' attendance to Royal Preston Hospital for surgery, having undergone at least 8 hours of pre-operative fasting. Blood samples were collected from all participants, with measurement of their serum CA125 levels. Ovarian cancer patients who received NACT had CA125 measurements at the time of their disease diagnosis as well. For this group, the mean interval between completion of their pre-operative chemotherapy and IDS was 39 days. Urine was collected from all participants apart from three controls. Table 1 contains epidemiological as well as CA125 data for the separate study groups. For each patient paired blood samples were obtained, one in tubes containing EDTA anticoagulant and one in serum gel tubes. Urine was collected following urethral cleansing and sterile urinary catheterisation without the use of lubricant gel. Blood samples were centrifuged at 2200 rpm for 15 min (local protocol), to obtain plasma and serum (which has the same content as plasma apart from clotting factors) from EDTA and serum gel tubes, respectively. This eliminated the presence of erythrocytes, which can interfere with spectra from important biomolecules. Plasmas and serums were subsequently snap frozen in liquid nitrogen and stored at -80°C. Urines were also stored at -80°C without centrifugation and snap freezing.

Prior to slide preparation, samples were thawed at room temperature. One ml from each urine sample was centrifuged at 2200 rpm for 15 min to eliminate the spectroscopic effect of possible contaminants (such as microorganisms and cellular material), and the supernatant was aspirated. Subsequently, 30 μl of individual biofluids (plama, serum and centrifuged urine) were deposited on glass slides covered with aluminium foil [33]. All slides were allocated a specific serial number for patient confidentiality. Following overnight drying, samples were transferred in wooden slide trays for Raman spectroscopic analysis. All slides were stored in de-humidified glass containers, to prevent sample condensation and physical damage. Ethical approval was granted by the East of England - Cambridge Central Research

Ethics Committee (Archival genito-urinary tissue, blood, urine, saliva and ascitic fluid collection; REC reference: 16/EE/0010; IRAS project ID: 195311).

Disease identification for all participants, as well as ovarian cancer staging, was based on histopathology reports after processing of surgical specimens. Tables 2 and 3 demonstrate staging data for the ovarian cancers and histological diagnoses for the entire cohort, respectively. Nearly all ovarian cancers were epithelial (66% with high-grade serous histology) and only one patient had a germ cell tumour. The International Federation of Gynecology and Obstetrics (FIGO) system was used for staging of ovarian malignancies [34]. 46% of non-chemotherapy ovarian cancer patients had early disease (FIGO I or II) and all NACT patients were at advanced stage (FIGO III or IV). Supplementary demographic data are available in non-patient identifiable databases.

Spectral acquisition

Raman spectra were obtained via a Renishaw InVia Basis spectrometer (Renishaw pls, UK) coupled to a Leica confocal microscope. A 200-mW laser diode was used at a 785 nm wavelength with a grating of 1200 lines/mm. Exposure time was set at 10 seconds, using 10% and 1% laser power for blood plasmas/serums and urines, respectively, with two accumulations at a spectral range between 2000 and 400 cm^{-1}. Ten point spectra were taken per sample, with a ×20 objective for laser beam focusing on the samples.

Computational analysis

All computational procedures were performed in the MATLAB R2014b version 8.4 environment (MathWorks, Inc., Natick, USA). Spectral pre-processing for data analysis consisted of: Savitzky-Golay (SG) smoothing (window of 51 points, 2^{nd} order polynomial fitting) and 2^{nd} derivative followed by vector normalisation. SG smoothing corrects for random noise, 2^{nd} derivative for baseline distortions, and vector normalisation for physical differences between samples such as thickness, light scattering and concentrations [35]. Exploratory and discriminant analyses were performed with the pre-processed and

mean-centred data. Principal component analysis (PCA) was used for exploratory analysis [36]. PCA reduces the pre-processed spectral dataset into a small number of principal components (PCs), responsible for the majority of data variance. Each PC is composed of scores and loadings; the former is used to access similarity/dissimilarity patterns among samples and the latter to identify spectral features (wavenumbers), associated with class separation and therefore possible spectral biomarkers [37]. Thus, the matrix containing the sample data with information about the sample classes is decomposed as follows:

$$\mathbf{X} = \mathbf{TP}^{\mathrm{T}} + \mathbf{E}$$

where X is the data matrix (i,j); T is the matrix of scores (i,A); P is the loading matrix (j,A); superscript T, as usual, indicates the transposition of a matrix; and E is the residual matrix (i,j), where i is the number of objects, j is the number of variables and A is the number of PCs used in the decomposition of the matrix. PCA models were built using the PLS Toolbox version 7.9.3 (Eigenvector Research, Inc., USA) and discriminant analysis was performed using the Classification Toolbox for MATLAB [38].

The genetic algorithm (GA) was also applied as a variable selection method. This is a non-deterministic method inspired by the theory of evolution. Its application generally aims to select the best variables for classification through an evolutionary process. Initially, a population of chromosomes is formed from the original variables. Then, an evaluation of the structures is made, and a further evolutionary process takes place. The optimised number of variables for GA was determined from the minimum cost function G, calculated for a given set of internal validations. This function is calculated as follows:

$$\mathrm{G} = \frac{1}{\mathrm{N_V}} \sum_{\mathrm{n}=1}^{\mathrm{N_V}} \mathrm{g_n}$$

where $\mathrm{g_n}$ is calculated as follows:

$$\mathrm{g_n} = \frac{\mathrm{r}^2(\mathrm{x_n}, \mathrm{m_{I(n)}})}{\min_{\mathrm{I(m)} \neq \mathrm{I(n)}} \mathrm{r}^2(\mathrm{x_n}, \mathrm{m_{I(m)}})}$$

where the numerator is the Mahalanobis distance (squared) between object x_n of class index I(n) and the sample mean $m_{I(n)}$ of its true class; and the denominator is the Mahalanobis distance (squared) between object x_n and the centre of the closest wrong class.

Linear discriminant analysis (LDA), quadratic discriminant analysis (QDA) and support vector machine (SVM) were used as classifiers. LDA and QDA are discriminant analysis methods based on the Mahalanobis distance between the analysed samples, where, as the main difference, a different variance structure is adopted by each model in relation to the analysed classes [39]. The first method assumes that both groups have similarity in terms of variance, while the second method assumes that the analysed classes have different variance structures, thus altering the calculation performed to determine the classes. The LDA score for the i-th sample of class k (L_{ik}) is calculated in non-Bayesian form as follows:

$$L_{ik} = (\mathbf{x}_i - \bar{\mathbf{x}}_k)^T \mathbf{C}_{\mathbf{pooled}}^{-1} (\mathbf{x}_i - \bar{\mathbf{x}}_k)$$

Similarly, the Q_{ik} score is calculated in non-Bayesian form as follows:

$$Q_{ik} = (\mathbf{x}_i - \bar{\mathbf{x}}_k)^{\mathbf{T}} \mathbf{C}_{\mathbf{k}}^{-1} (\mathbf{x}_i - \bar{\mathbf{x}}_k)$$

where $\mathbf{x}_i$ is a vector with the input variables for sample i; $\bar{\boldsymbol{x}}_k$ is the mean of class k; C_{pooled} is the pooled covariance matrix between the classes.

SVM is a non-linear data classifier. Thus, it seeks to find a classification hyperplane that provides the greatest margin of separation between data groups. During modelling, data are transformed into a space with different characteristics through a core function in the algorithm, which is largely responsible for optimisation of results. The most widely used kernel function for classification, as performed herein, is the radial basis function (RBF) [35, 40]. The RBF function is calculated as follows:

$$k(\mathbf{x}_i, \mathbf{z}_j) = \exp(-\gamma \|\mathbf{x}_i - \mathbf{z}_j^2\|)$$

where x_i and z_j are sample measurement vectors and γ is a tuning parameter that controls the RBF window parameter. In this study, this parameter was set to 1. The SVM classification rule is obtained by the following equation:

$$f(x) = \text{sign}\left(\sum_{i=1}^{Nsv} \alpha_i\, y_i \kappa(\mathbf{x}_i, \mathbf{z}_j) + b\right)$$

where N_{SV} is the number of support vectors; α_i is the multiplier of Lagrange; y_i is the affiliation of the respective analysed class ($\pm$ 1); $k(x_i, z_j)$ is the kernel function and b is the polarisation parameter. These parameters are obtained by a set of samples validation.

Furthermore, partial least squares discriminant analysis (PLS-DA) was also used as a comparative technique. PLS-DA is one of the most popular supervised classification techniques, based on a linear model for which the classification criterion is obtained by PLS [41]. In PLS-DA, PLS is applied to data reducing the original variables (wavenumbers) to a few numbers of latent variables in an iterative process, where the class labels for each sample are known in the training set. Then, a straight line that divides the classes' regions is found [42].

Statistical analysis

The discriminant models were evaluated by calculating some metrics (accuracy, sensitivity, specificity and F-score) in the test set, composed of 30% of samples selected by using the Morais-Lima-Martin (MLM) algorithm [43]. Training samples, composed of 70% of the dataset, were used for model construction *via* training and cross-validation {for sample splitting methodology see Electronic Supplementary Information (ESI) Table S1}. The accuracy represents the total number of samples correctly classified considering true and false negatives, the sensitivity represents the proportion of positives (*i.e.*, ovarian cancers spectra) correctly identified, the specificity represents the proportion of negatives (*i.e.*, benign controls spectra) correctly identified, and the F-score measures the overall model performance considering imbalanced data [44]. These parameters are calculated as follows:

$$\text{Accuracy}\ (\%) = [(TP + TN)/(TP + FP + TN + FN)] \times 100$$

$$\text{Sensitivity}\ (\%) = [TP/(TP + FN)] \times 100$$

$$\text{Specificity}\ (\%) = [TN/(TN + FP)] \times 100$$

$$\text{F-score}\ (\%) = (2 \times \text{SENS} \times \text{SPEC})/(\text{SENS} + \text{SPEC})$$

where TP stands for true positives, TN for true negatives, FP for false positives and FN for false negatives. SENS stands for sensitivity and SPEC for specificity.

P-values were calculated for two-dimensional PCA score plots using a MANOVA test and for individual wavenumbers based on an ANOVA test. Statistical significance was considered at $P < 0.05$ and statistical high significance at $P < 0.001$.

Results and Discussion

Vibrational spectroscopy employs powerful tools to obtain information about biological materials. Herein, Raman spectroscopy was applied to identify the potential of plasma, serum and urine towards ovarian cancer diagnosis. The majority of peaks produced by inelastic scattering of biomolecules is located at the so called ‘’fingerprint’’ region of the spectrum, between 500 - 1750 cm^{-1} wavelengths [45], and consisted the area of focus for spectrochemical analyses in this study. Patient cohorts, including ovarian cancers with several different histological sub-types and stages, and benign controls with variable gynaecological pathologies, provided a realistic approach to clinical settings. Furthermore, the strategy used in recruitment of participants (consecutive enrolment) ensured elimination of patient selection bias.

An initial exploratory analysis was conducted to check for possible significant spectral variations between two subgroups in each of the study’s main cohorts (Figure 1). For controls, this comparison involved patients with endometriosis (which has a propensity towards ovarian malignancy) [46] and patients with all other benign conditions. PCA scores identified no difference in any biofluid (*P*-values >0.2). The opposite was observed in comparisons between ovarian cancer patients without previous chemotherapy and post-NACT, where statistically significant differences for all biofluids (*P*-values 0.02 - 0.0005) indicated a potential effect of chemotherapy on spectra. Therefore, these subgroups were

compared separately against the whole cohort of controls. Raw and mean raw spectra of benign control and ovarian cancer classes are presented in ESI Figures S1 and S2, respectively.

ESI Figures S3 and S4 demonstrate raw and mean raw spectra, respectively, of the two distinct ovarian cancer classes in relation to controls; their pre-processed and mean pre-processed spectra are presented in Figure 2 and ESI Figure S5, respectively. PCA score plots from the comparison of non-chemotherapy ovarian cancer patients *versus* benign ones demonstrated high statistically significant differences only in plasma ($P \approx 0.001$; Figure 3). However, this was not reflected on the sensitivities obtained with five classification algorithms, where only one (GA-QDA) demonstrated a fair potential for identification of ovarian cancer (73% sensitivity), with the rest ranging between 32% - 61%. As anticipated from the PCA scores, outcomes were even worse for serum and urine, with sensitivities ranging between 33% - 58% and 0% - 45%, respectively. On the other hand, high specificities and accuracies were generally obtained in all biofluids, the vast majority being above 85% (range 37% - 100%) for the former and above 75% (range 39% - 88%) for the latter (see ESI Table S2).

Opposite findings were observed at the PCA scores from comparisons between NACT ovarian cancer patients and controls, where statistically significant differences are noted in serum ($P = 0.004$) and urine ($P = 0.0007$) but not in plasma ($P = 0.06$) (Figure 3). As expected, obtained sensitivities for the latter were markedly lower in most classification algorithms compared to the ones for the non-chemotherapy ovarian cancer group. Even in the single algorithm (PLS-DA) that showed a significant opposite trend (with a rise in sensitivity from 59% to 100%), specificity and accuracy dropped considerably (from 90% to 54% and from 84% to 60%, respectively), suggesting the presence of spectral similarities between NACT ovarian cancers and controls. Interestingly, despite initial findings at the PCA scores, all classification algorithms in serum also demonstrated markedly lower sensitivities for identification of the post-NACT ovarian cancer group compared to the non-chemotherapy one, whereas high specificities and accuracies were maintained (see ESI Table S2). Taken together, these findings suggest a trend towards a more ‘’benign’’ pattern in Raman spectra acquired from blood-derived biofluids following neo-adjuvant chemotherapy,

which is reported for the first time. They also correlate well with the degree of chemosensitivity exhibited by our NACT patients, based on an overall substantial drop in serum CA125 at the time of IDS compared to baseline levels (Table 1), a reduction in tumour load at their interval computed tomography scan and a chemotherapy response score (CRS) of 2 or 3 (*i.e.* appreciable or complete response) [47] in 75% of them, following histopathological assessment of surgically excised tissues.

PLS-DA was overall the algorithm with the best performance in comparisons between ovarian cancer groups and controls (as indicated by the relevant F-scores; see ESI Table S2) and its statistical metrics are presented in Table 4. Therefore, discriminant function plots on training and test samples (Figure 4), as well as regression coefficient plots for identification of key biomarkers (ESI Figure S6), were produced from this algorithm. Spectral wavenumbers assigned to peaks in the latter plots represent molecular classifiers between different groups, and their intensity indicates the magnitude of inter-class differences for a specific biomarker. In plasma and serum, the majority of ‘’strong’’ absorbance intensities in comparisons between non-chemotherapy ovarian cancers and controls can be allocated to structural components of mucins, which belong to the family of glycoproteins. More specifically, observed peaks at approximate wavelengths 880, 950, 1000, 1380, 1600 and 1680 cm^{-1} can be assigned either to carbohydrate moieties (such as galactosamine, glucosamine, galactose) or amino acids (such as serine, threonine) that are rich in mucins [48-50]. Interestingly, most of these peaks were common in the regression coefficient plots of plasma and serum, and almost all suggested more abundant presence of these constituents in ovarian cancers. Among other mucins (such as mucin 1 - the cancer antigen CA15-3), detected in blood of patients with ovarian cancer and benign gynaecological pathologies, CA125 (also known as mucin 16) has by far the largest molecular weight (due to its heavier glycosylation and lengthier protein backbone). It also exhibits the widest concentration differences between ovarian malignancy and non-malignant states [51-53]. Therefore, CA125 is likely to be the main contributor to absorbances in the aforementioned spectral wavelengths. Remarkably, peaks at these wavelengths were also observed at comparisons between NACT patients and controls both in plasma and serum, but

regression coefficients were generally smaller compared to the non-chemotherapy ovarian cancer group. This correlates with the observed magnitude of differences in mean CA125 levels between each of these two groups and controls (Table 1), and reinforces our impression about a potential of Raman spectroscopy to detect chemotherapy related effects in ovarian cancer. Of note, these variances in absorbance intensities were more pronounced in plasma than serum, which could account for the overall wider differences in statistical metrics between the two ovarian cancer classes observed at the former (see ESI Table S2).

On the other hand, peaks at wavelength areas 1420 - 1450, 1650 and 1750 cm^{-1} were either higher at the NACT group or had negative regression coefficients with stronger absorbances at the non-chemotherapy ovarian cancers in comparisons with controls. All these bands are assigned to lipids [54] and these intensity differences were observed both in plasma and serum, suggesting an increase in blood lipid levels post-NACT. Interestingly, platinum and taxane chemotherapy has been associated with hyperlipidaemia in testicular and breast carcinomas, respectively [55, 56]. Malignant cells are known to use high amounts of lipids for their energy demands and accelerated consumption has been associated with chemoresistance in ovarian cancer [56, 57]. Therefore, higher blood lipid levels might be an indirect measure of treatment response, reflecting a decrease in this metabolic activity with decelerated tumour growth. Although other parameters may have affected these changes (such as pre-treatment cachexia and improved appetite post-NACT leading to higher lipid intake), spectral changes at the aforementioned wavelengths could exhibit potential for monitoring response to chemotherapy in ovarian cancer.

In urine, statistical metrics for diagnosis of ovarian cancer in the non-chemotherapy group were lower compared to blood-derived biofluids. This could be attributed to weaker absorbances observed in bands allocated to mucins and correlates with the markedly low urinary CA125 concentrations, with much smaller mean differences between patients with ovarian cancer and benign gynaecological conditions than those present in blood [58, 59]. However, contrary to plasma and serum, statistical metrics in nearly all classification algorithms were higher for NACT patients, with consistently higher sensitivities

(reaching 100% in PLS-DA). As expected, regression coefficients at wavelengths associated with mucins' components were generally even lower in this group, indicating that different biomolecules were the main classifiers in comparisons with controls (see ESI Table S2, Figure S6).

Indeed, the peak exhibiting the strongest intensity (with regression coefficient >0.6) is located at 1030 cm^{-1} and is assigned to collagen [54]. In ovarian cancer, marked degradation of collagen present in peritoneal surfaces is known to occur during the formation of metastases, and collagen peptides are found in the urine of patients with ovarian malignancies [60, 61]. The drop in this peak's regression coefficient at the non- chemotherapy group (regression coefficient <0.3) is likely to reflect the higher number of patients with advanced metastatic ovarian cancer in the NACT cohort, and a similar trend was observed in plasma and serum. Its appearance as a strong classifier in urine may be due the latter's less complex protein profile than blood [62], making it a potential candidate for monitoring response to chemotherapy in patients with widely disseminated (FIGO stage IIIC or IV) ovarian cancer.

The same wavelength area (1030 - 1040 cm^{-1}) contains peaks at the Raman spectrum of polyamines (spermine, spermidine), which are low molecular weight molecules participating in cellular proliferation and DNA synthesis [63]. Interestingly, in ovarian cancer, urinary excretion of polyamines increases after platinum-based chemotherapy, but this effect is mostly observed in chemo-sensitive disease [64]. Another band demonstrating strong absorbance at the post-chemotherapy group is located at 970 cm^{-1}, assigned to phosphorylated proteins [54]. Its peak had a more intense negative regression coefficient (nearly 0.6) at these patients compared to non-chemotherapy ones (regression coefficient = 0.2), suggesting more attenuated expression at the former compared to controls. A phosphoprotein exhibiting reduced urinary excretion following administration of several chemotherapy agents (including platins) is osteopontin, also known as secreted phosphoprotein 1, which is involved in cell-matrix interactions [65, 66]. Whether chemotherapy-related alterations at the aforementioned wavelengths can be specifically attributed to these molecules should be addressed in future studies, particularly since osteopontin and acetylated spermine have both been proposed as possible urinary biomarkers for ovarian cancer diagnosis [67].

Contrary to what was observed in plasma and serum, absorbances at the 1420 - 1450 and 1750 cm^{-1} wavelengths (produced as previously stated by bonds in lipids) were more intense at the non-chemotherapy ovarian cancer group compared to NACT patients, and had positive regression coefficients at the former. There is a lack of studies investigating the effect of chemotherapy in urinary lipid concentrations, although significantly lower phospholipids in urine of breast cancer patients have been reported post surgical treatment (*i.e.*, after partial or complete elimination of tumour load) [68]. Therefore, differential absorbance trends at these wavelengths in blood and urine might also consist benchmarks for monitoring NACT response in ovarian cancer.

Our study is the first to explore the potential of Raman spectroscopy of urine in ovarian cancer diagnosis, and the first to attempt identification of chemotherapy effects in ovarian malignancies with this spectroscopic technique, both in blood and urine biofluids. Three studies have previously assessed the performance of blood plasma or serum Raman spectroscopy towards ovarian cancer detection. All compared equal numbers of ovarian cancer cases and controls with benign gynaecological conditions, excluding patients who had received chemotherapy, and all used only one classification algorithm (SVM) in comparisons [30-32]. In the largest previous study by Paraskevaidi *et al.* (27 ovarian cancer patients), both spontaneous Raman and surface enhanced Raman spectroscopy (SERS - a technique used to increase the inherently weak Raman signal) were applied to blood plasma. Sensitivities and specificities for the former were 94% and 96%, whereas for the latter 87% and 89%, respectively. In their cohort, 63% of ovarian cancer patients had FIGO stage I disease compared to 37% in our study for the non-chemotherapy group [30]. In the smallest study by Owens *et al.* (2 ovarian cancer patients), a classification accuracy of 74% for plasma was obtained [31]. Finally, in the study by Ullah *et al.* (11 ovarian cancer patients), Raman spectroscopy of serum demonstrated 90% sensitivity and 100% specificity [32]. In our study, application of five different classification algorithms achieved similar or higher specificities and accuracies but lower sensitivities. These variations are probably due to the much bigger size of our cohort (10 - 100 times compared to the aforementioned studies) which increased patient

heterogeneity, but at the same time provides a more pragmatic estimate of Raman spectroscopy's performance towards ovarian cancer diagnosis in the general population. The influence of epidemiological factors (such as age, BMI, comorbidities) in differential outcomes could not be determined, as none of these studies (including ours) performed regression analyses for these variables.

Paraskevaidi *et al.* also assessed the performance of blood plasma Raman spectroscopy in relation to serum CA125 measurements, using the cut-off threshold of 35 u/ml to discriminate between normal and elevated levels [30]. Interestingly, both spontaneous Raman and SERS exhibited more than 20% drop in sensitivity at the patient subgroup with CA125 levels <35 u/ml, strengthening our impression that this mucin consists a major classifier for ovarian cancer diagnosis through Raman spectroscopy. Another remarkable observation is the presence of common peaks between our study and the aforementioned ones. More specifically, absorbance intensities at all previously highlighted wavelength areas in plasma and serum were also present either in the study by Paraskevaidi *et al.* or in the one by Ullah *et al* [30, 32]. As these bands were mainly assigned to structural components of mucins and lipids, their repeated emergence as key biomarkers highlights their importance in discriminating between ovarian cancer and benign gynaecological conditions with Raman spectroscopy, confirming at the same time reproducibility of our results.

The performance of several serum biomarkers in the detection of ovarian malignancies has been extensively investigated. CA125 and HE4 are the most frequently explored, achieving sensitivities and specificities up to 82% and 93%, respectively, when assessed either remotely or in combination [69, 70]. Additionally, ultrasound-based predictive models with or without incorporation of CA125 levels, have demonstrated sensitivities up to 93% and specificities up to 92% [71]. In our study, Raman spectroscopy of biofluids exhibited overall lower sensitivities for diagnosis of ovarian cancer without previous treatment. On the other hand, plasma and serum obtained high specificities (≥90%) and very good accuracies (≥85%) with most classification algorithms. Compared to serum assays, Raman spectroscopy of blood-derived biofluids is more cost-effective (as it does not require the use of reagents) and time-

efficient (producing results in minutes instead of hours or days). Furthermore, the avoidance of discomfort and intimacy associated with transvaginal ultrasonography is likely to result in higher patient satisfaction and acceptance rates. Taking all the above into consideration, Raman spectroscopy of blood plasma or serum could be used as a point-of-care test to rule out ovarian cancer in patients presenting with suspicious symptoms.

The main strengths of this study is the size of its cohort (the biggest employed so far in Raman spectroscopy of biofluids for ovarian cancer detection), along with its prospective design and consecutive recruitment of participants. In this field, it presents the first concurrent comparison of three different biofluids. The inclusion of patients with a wide range of benign gynaecological conditions, as well as various ovarian cancer histological sub-types and stages, provides a pragmatic approach to the encounter of these entities in the general population. It is also the first study assessing the potential of biofluids' Raman spectroscopy to detect chemotherapy-related changes in ovarian cancer treatment, and a possible correlation of these alterations with prediction of chemosensitivity. Weaknesses include not evaluating the impact of confounding factors on outcomes and performance in early stage disease detection, which is the main challenge in the timely diagnosis of ovarian cancer. These parameters would restrict direct clinical application of blood plasma and serum Raman spectroscopy as diagnostic tools in ovarian malignancies. Additionally, the assessment of chemotherapy effects was not conducted on a single ovarian cancer patient group with samples collection pre- and post-NACT, and therefore relevant results consist a rather preliminary indirect manifestation about the potential of vibrational spectroscopy in evaluating treatment response.

In conclusion, our study has rationalised previously reported performance of blood-derived biofluids' Raman spectroscopy in the diagnosis of ovarian cancer, and offers a novel assessment of urine towards this direction. All three examined biofluids exhibited potential for identifying chemotherapy-related spectrochemical changes, which in plasma and serum can be partially attributed to variable levels of the tumour marker CA125. These results require validation by future research, with linear follow-up of a

unique ovarian cancer cohort before and after NACT, and an attempt for correlations with tumour resectability at IDS as well as survival outcomes. As different ovarian cancer subtypes can exhibit varied levels of chemosensitivity, it would also be of interest to explore whether these can be assessed by Raman spectroscopy, through comparisons between distinct histological groups. Finally, future studies applying different spectroscopic techniques (such as infrared methods) should explore whether the potential of vibrational spectroscopy towards ovarian cancer diagnosis can be optimised, or whether Raman spectroscopy can perform better in classification of separate histological sub-types as opposed to a mixed ovarian cancer cohort; the latter should ideally be addressed in large prospective multi-centre trials, in order to achieve adequate numbers of patients for these subgroup analyses, which were not available herein.

Acknowledgements

The authors thank the patients and staff of Royal Preston Hospital for facilitating these studies, with special thanks to our Research Technician Katherine M. Ashton. We would also like to thank Camilo L. M. Morais, PhD, for his advice during the course of this study. Funding from Rosemere Cancer Foundation is gratefully acknowledged. D. L. D. Freitas would like to thank the Coordenação de Aperfeiçoamento de Pessoal de Nível Superior (CAPES), Brazil, for his research grant. R. V. O. Silva would like to thank the Conselho Nacional de Desenvolvimento Científico e Tecnológico (CNPq), Brazil, for her research grant.

Ovarian cancers	**Mean [Range]**
Age	
All patients (*n*=116)	63 [20-84]
No NACT (*n*=71)	61 [20-84]
NACT (*n*=45)	65 [43-83]
BMI (kg/m^2)	
All patients (*n*=116)	26.7 [16.6-48.6]
No NACT (*n*=71)	27.4 [18.2-48.6]
NACT (*n*=45)	25.8 [16.6-36.4]
CA125 (u/ml)	
Non-chemotherapy group (*n*=71)	590 [5-8366]
Chemotherapy group, pre-NACT (*n*=45)	2595 [62-23455]
Chemotherapy group, post-NACT (*n*=45)	135 [8-1104]
Benign controls (*n*=307)	
Age	47 [19-89]
BMI (kg/m^2)	28.5 [17.3-49.8]
CA125 (u/ml)	55 [1-2627]

Table 1: Epidemiological and serum CA125 data for the different study groups. CA125 level was considered elevated if measuring >35 u/ml. NACT: neo-adjuvant chemotherapy.

	Non NACT	NACT
IA	10	-
IC	16	-
IIA	5	-
IIB	2	-
IIIA	5	-
IIIB	4	1
IIIC	27	36
IVA	2	5
IVB	-	3

Table 2: FIGO staging of ovarian cancer patients. NACT: neo-adjuvant chemotherapy.

	No of patients	
Ovarian cancers	No NACT	NACT
High grade serous	33	43
Low grade serous	5	-
Primary peritoneal serous	-	1
Mucinous	10	-
Endometrioid	9	-
Clear cell	8	-
Carcinosarcoma	4	1
Anaplastic	1	-
Immature teratoma	1	-
Benign controls		
Ovarian cysts (non-endometriomas)		
Cystadenomas, fibromas, cystadenofibromas	71	
Mature cystic teratomas	13	
Follicular	3	
Haemorrhagic	2	
Struma ovarii	2	
Brenner	1	
Sertoli-Leydig	1	
Indeterminate	2	
Endometriosis (including endometriomas)		
Stage 1	16	
Stage 2	9	
Stage 3	19	
Stage 4	28	
Uterine fibroids and / or adenomyosis	69	
Pelvic inflammatory disease	9	
Endometrial / cervical polyps	8	
Hydrosalpinx / paratubal cysts	7	
Uterine prolapse	3	
Peritoneal leiomyomatosis	1	
Endometrial hyperplasia	1	
Cervical intraepithelial neoplasia (CIN)	1	
Normal (no pathology identified)	41	

Table 3: Histopathological data for the entire cohort. Staging of endometriosis patients was based on intra-operative findings according to the American Society of Reproductive Medicine staging system [72]. NACT: neo-adjuvant chemotherapy.

	Plasma		Serum		Urine	
	OC no chemo	**OC with chemo**	**OC no chemo**	**OC with chemo**	**OC no chemo**	**OC with chemo**
Sensitivity	59%	100%	57%	43%	45%	100%
Specificity	90%	54%	93%	82%	85%	87%
Accuracy	84%	60%	87%	76%	77%	89%

Table 4: PLS-DA statistical metrics in classification of the two ovarian cancer groups (non-chemotherapy - OC no chemo, NACT - OC with chemo) from benign controls for plasma, serum and urine. OC: ovarian cancers, chemo: chemotherapy, NACT: neo-adjuvant chemotherapy.

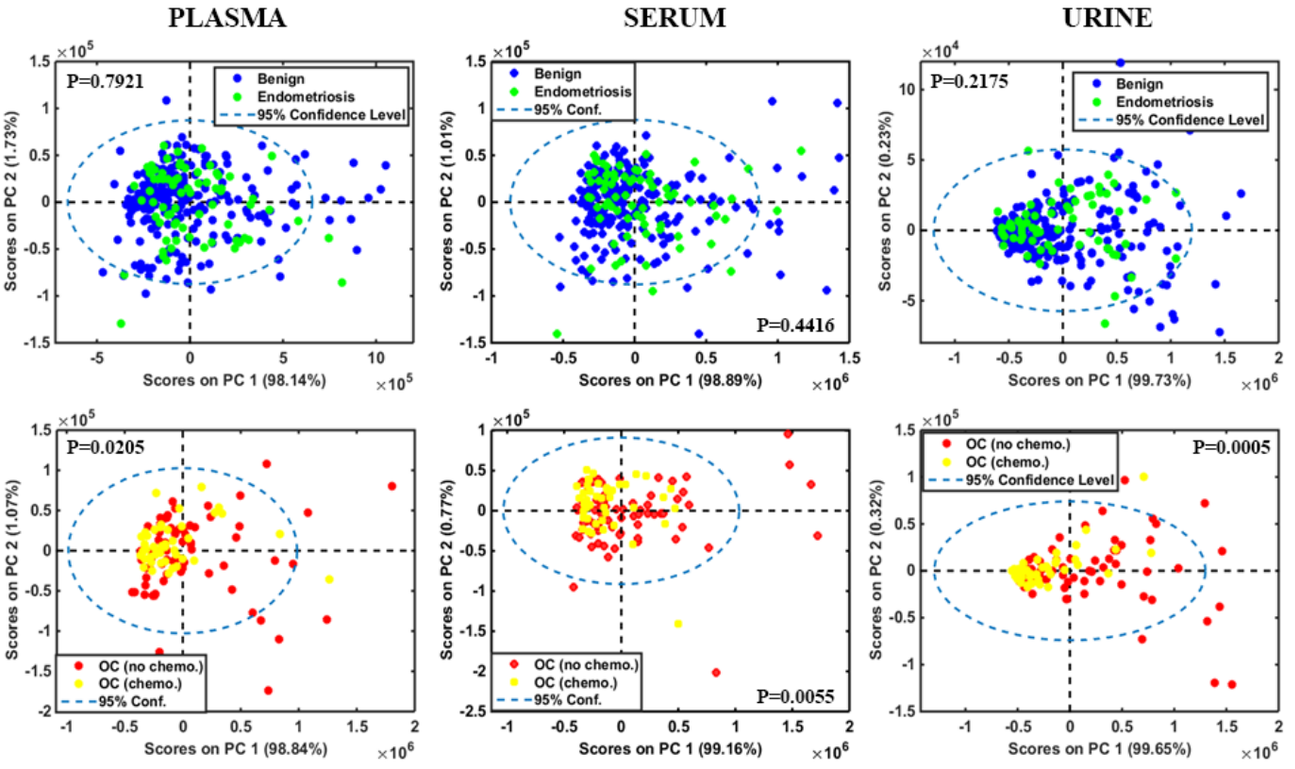

Figure 1: PCA score plots with *P*-values for intra-class comparisons in plasma, serum and urine. Top graphs: non-endometriosis (benign) *versus* endometriosis benign controls. Bottom graphs: non-chemotherapy (OC no chemo) *versus* NACT (OC chemo) ovarian cancer patients. OC: ovarian cancers, chemo: chemotherapy, NACT: neo-adjuvant chemotherapy

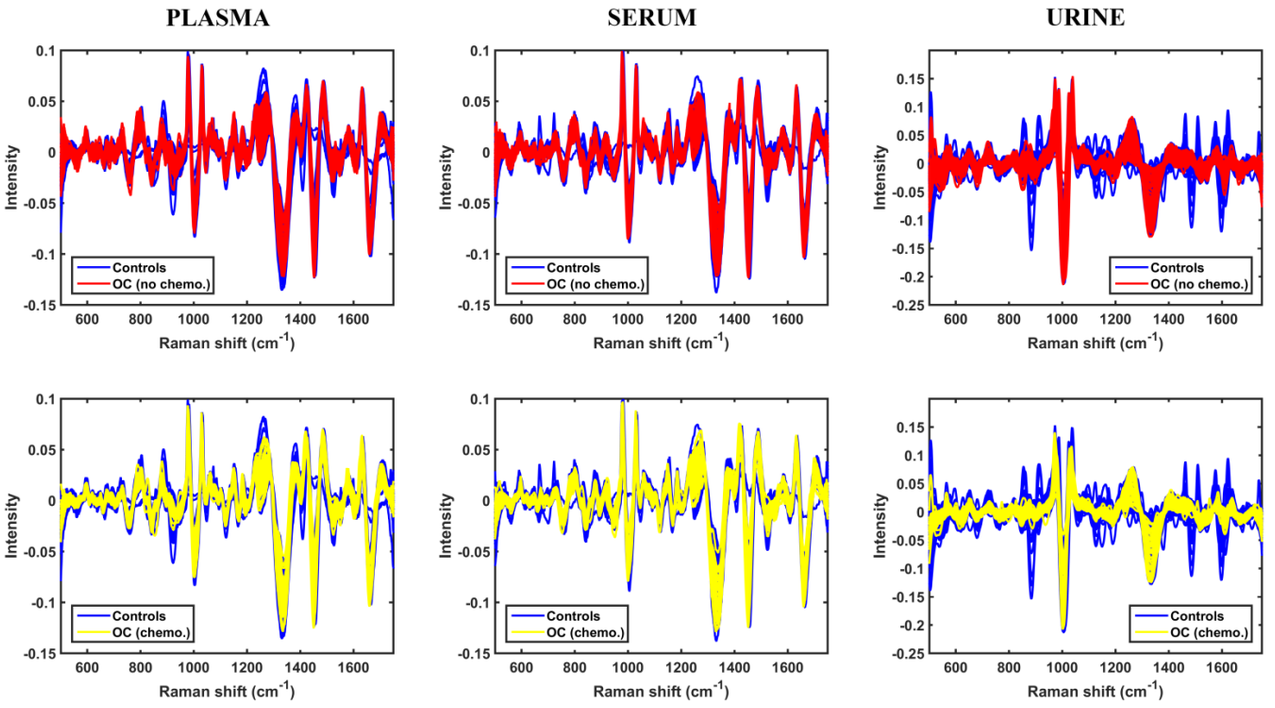

Figure 2: Pre-processed spectra of ovarian cancer classes *versus* all benign controls for plasma, serum and urine. Top graphs: non-chemotherapy ovarian cancers (OC no chemo) *versus* controls. Bottom graphs: NACT ovarian cancers (OC chemo) *versus* controls. OC: ovarian cancers, chemo: chemotherapy, NACT: neo-adjuvant chemotherapy

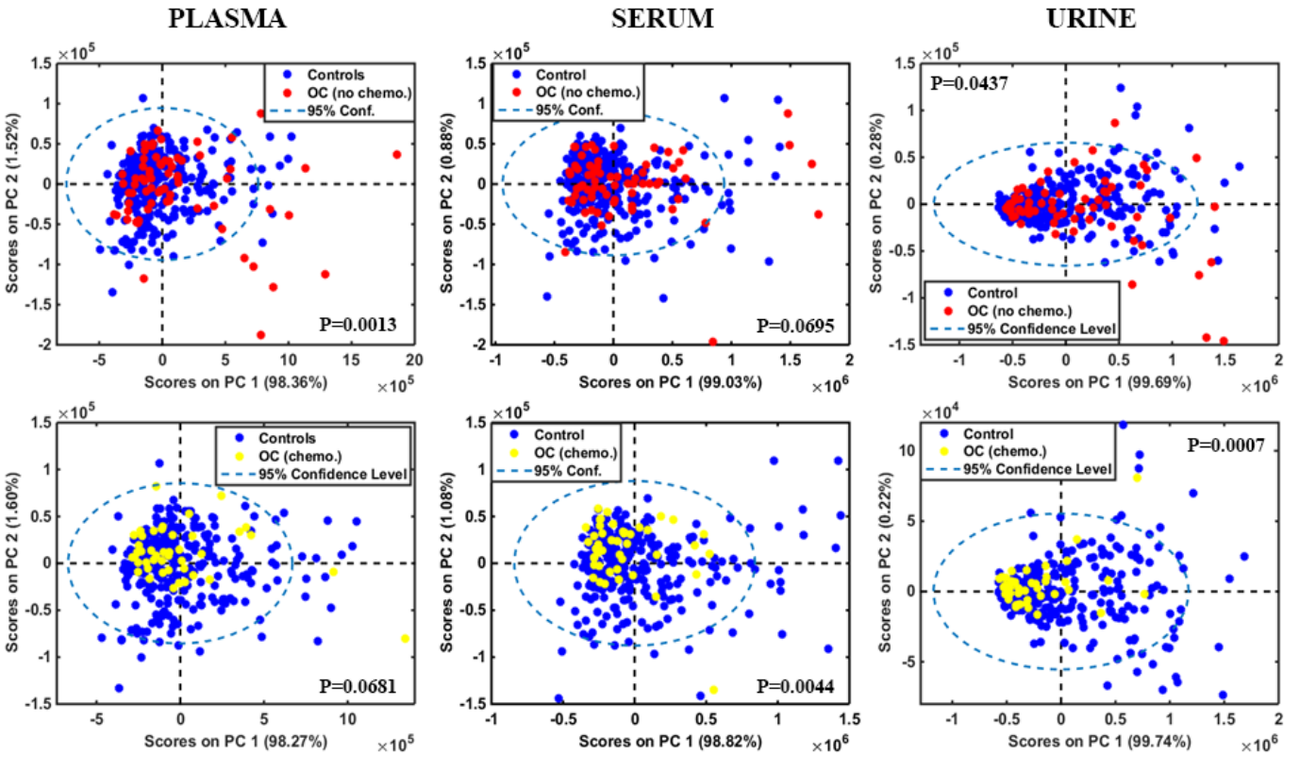

Figure 3: PCA score plots with *P*-values for inter-class comparisons in plasma, serum and urine. Top graphs: non-chemotherapy ovarian cancers (OC no chemo) *versus* all benign controls (controls). Bottom graphs: NACT ovarian cancers (OC chemo) *versus* all benign controls (controls). OC: ovarian cancers, chemo: chemotherapy, NACT: neo-adjuvant chemotherapy

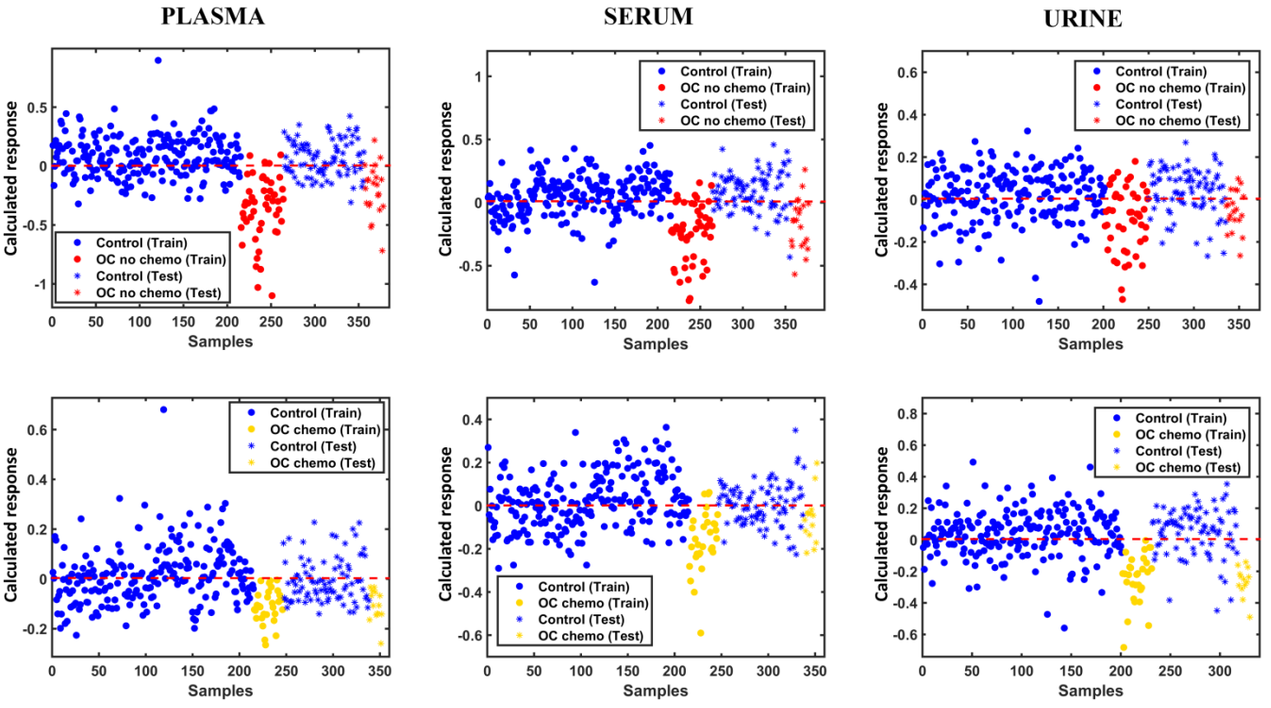

Figure 4: PLS-DA discriminant function plots for plasma, serum and urine. Top graphs: non-chemotherapy ovarian cancers (OC no chemo) *versus* all benign controls (controls). Bottom graphs: NACT ovarian cancers (OC chemo) *versus* all benign controls (controls). OC: ovarian cancers, chemo: chemotherapy, NACT: neo-adjuvant chemotherapy

Data Availability Statement

The raw spectra used in this study are openly available in the data repository ‘’Figshare’’ at: https://doi.org/10.6084/m9.figshare.14562312.

Reference: P. Giamougiannis, P. L. Martin-Hirsch, F. L. Martin. 2021. Figshare.

References

[1] F. Bray, J. Ferlay, I. Soerjomataram, R. L. Siegel, L. A. Torre, A. Jemal. CA Cancer J Clin. 2018, 68, 394.

[2] F. Reid. International Agency for Research on Cancer. 2018.

[3] C. Stewart, C. Ralyea, S. Lockwood. Semin Oncol Nurs. 2019, 35, 151.

[4] U. A. Matulonis, A. K. Sood, L. Fallowfield, B. E. Howitt, J. Sehouli, B. Y. Karlan. Nat Rev Dis Primers. 2016, 2, 16061.

[5] S. Lheureux, C. Gourley, I. Vergote, A. M. Oza. Lancet. 2019, 393, 1240.

[6] I. J. Jacobs, U. Menon, A. Ryan, A. Gentry-Maharaj, M. Burnell, J. K. Kalsi, N. N. Amso, S. Apostolidou, E. Benjamin, D. Cruickshank, D. N. Crump, S. K. Davies, A. Dawnay, S. Dobbs, G. Fletcher, J. Ford, K. Godfrey, R. Gunu, M. Habib, R. Hallett, J. Herod, H. Jenkins, C. Karpinskyj, S. Leeson, S. J. Lewis, W. R. Liston, A. Lopes, T. Mould, J. Murdoch, D. Oram, D. J. Rabideau, K. Reynolds, I. Scott, M. W. Seif, A. Sharma, N. Singh, J. Taylor, F. Warburton, M. Widschwendter, K. Williamson, R. Woolas, L. Fallowfield, A. J. McGuire, S. Campbell, M. Parmar, S. J. Skates. Lancet. 2016, 387, 945.

[7] S. S. Buys, E. Partridge, A. Black, C. C. Johnson, L. Lamerato, C. Isaacs, D. J. Reding, R. T. Greenlee, L. A. Yokochi, B. Kessel, E. D. Crawford, T. R. Church, G. L. Andriole, J. L. Weissfeld, M. N. Fouad, D. Chia, B. O'Brien, L. R. Ragard, J. D. Clapp, J. M. Rathmell, T. L. Riley, P. Hartge,

P. F. Pinsky, C. S. Zhu, G. Izmirlian, B. S. Kramer, A. B. Miller, J. L. Xu, P. C. Prorok, J. K. Gohagan, C. D. Berg. JAMA. 2011, 305, 2295.

[8] I. Jacobs, D. Oram, J. Fairbanks, J. Turner, C. Frost, J. G. Grudzinskas. Br J Obstet Gynaecol. 1990, 97, 922.

[9] R. G. Moore, D. S. McMeekin, A. K. Brown, P. DiSilvestro, M. C. Miller, W. J. Allard, W. Gajewski, R. Kurman, R. C. Bast, Jr., S. J. Skates. Gynecol Oncol. 2009, 112, 40.

[10] A. Aithal, S. Rauth, P. Kshirsagar, A. Shah, I. Lakshmanan, W. M. Junker, M. Jain, M. P. Ponnusamy, S. K. Batra. Expert Opin Ther Targets. 2018, 22, 675.

[11] H. Meden, A. Fattahi-Meibodi. Int J Biol Markers. 1998, 13, 231.

[12] F. L. Martin. Nature Methods. 2011, 8, 385.

[13] H. J. Butler, L. Ashton, B. Bird, G. Cinque, K. Curtis, J. Dorney, K. Esmonde-White, N. J. Fullwood, B. Gardner, P. L. Martin-Hirsch, M. J. Walsh, M. R. McAinsh, N. Stone, F. L. Martin. Nature Protocols. 2016, 11, 664.

[14] J. G. Kelly, J. Trevisan, A. D. Scott, P. L. Carmichael, H. M. Pollock, P. L. Martin-Hirsch, F. L. Martin. Journal of Proteome Research. 2011, 10, 1437.

[15] M. J. Baker, S. R. Hussain, L. Lovergne, V. Untereiner, C. Hughes, R. A. Lukaszewski, G. Thiefin, G. D. Sockalingum. Chemical Society Reviews. 2016, 45, 1803.

[16] H. F. Nargis, H. Nawaz, A. Ditta, T. Mahmood, M. I. Majeed, N. Rashid, M. Muddassar, H. N. Bhatti, M. Saleem, K. Jilani, F. Bonnier, H. J. Byrne. Spectrochim Acta A Mol Biomol Spectrosc. 2019, 222, 117210.

[17] J. L. Pichardo-Molina, C. Frausto-Reyes, O. Barbosa-García, R. Huerta-Franco, J. L. González-Trujillo, C. A. Ramírez-Alvarado, G. Gutiérrez-Juárez, C. Medina-Gutiérrez. Lasers Med Sci. 2007, 22, 229.

[18] D. K. R. Medipally, D. Cullen, V. Untereiner, G. D. Sockalingum, A. Maguire, T. N. Q. Nguyen, J. Bryant, E. Noone, S. Bradshaw, M. Finn, M. Dunne, A. M. Shannon, J. Armstrong, A. D. Meade, F. M. Lyng. Ther Adv Med Oncol. 2020, 12, 1758835920918499.

[19] G. Del Mistro, S. Cervo, E. Mansutti, R. Spizzo, A. Colombatti, P. Belmonte, R. Zucconelli, A. Steffan, V. Sergo, A. Bonifacio. Anal Bioanal Chem. 2015, 407, 3271.

[20] S. Li, L. Li, Q. Zeng, Y. Zhang, Z. Guo, Z. Liu, M. Jin, C. Su, L. Lin, J. Xu, S. Liu. Sci Rep. 2015, 5, 9582.

[21] H. M. Huttanus, T. Vu, G. Guruli, A. Tracey, W. Carswell, N. Said, P. Du, B. G. Parkinson, G. Orlando, J. L. Robertson, R. S. Senger. PLoS One. 2020, 15, e0237070.

[22] I. Maitra, C. L. M. Morais, K. M. G. Lima, K. M. Ashton, R. S. Date, F. L. Martin. J Biophotonics. 2020, 13, e201960132.

[23] M. Bahreini, A. Hosseinzadegan, A. Rashidi, S. R. Miri, H. R. Mirzaei, P. Hajian. Talanta. 2019, 204, 826.

[24] M. Tatarkovič, M. Miškovičová, L. Šťovíčková, A. Synytsya, L. Petruželka, V. Setnička. Analyst. 2015, 140, 2287.

[25] C. A. Jenkins, R. A. Jenkins, M. M. Pryse, K. A. Welsby, M. Jitsumura, C. A. Thornton, P. R. Dunstan, D. A. Harris. Analyst. 2018, 143, 6014.

[26] I. Taleb, G. Thiéfin, C. Gobinet, V. Untereiner, B. Bernard-Chabert, A. Heurgué, C. Truntzer, P. Hillon, M. Manfait, P. Ducoroy, G. D. Sockalingum. Analyst. 2013, 138, 4006.

[27] L. Habartová, B. Bunganič, M. Tatarkovič, M. Zavoral, J. Vondroušová, K. Syslová, V. Setnička. Chirality. 2018, 30, 581.

[28] J. L. González-Solís, J. C. Martínez-Espinosa, L. A. Torres-González, A. Aguilar-Lemarroy, L. F. Jave-Suárez, P. Palomares-Anda. Lasers Med Sci. 2014, 29, 979.

[29] S. Feng, D. Lin, J. Lin, B. Li, Z. Huang, G. Chen, W. Zhang, L. Wang, J. Pan, R. Chen, H. Zeng. Analyst. 2013, 138, 3967.

[30] M. Paraskevaidi, K. M. Ashton, H. F. Stringfellow, N. J. Wood, P. J. Keating, A. W. Rowbottom, P. L. Martin-Hirsch, F. L. Martin. Talanta. 2018, 189, 281.

[31] G. L. Owens, K. Gajjar, J. Trevisan, S. W. Fogarty, S. E. Taylor, B. Da Gama-Rose, P. L. Martin-Hirsch, F. L. Martin. J Biophotonics. 2014, 7, 200.

[32] I. Ullah, I. Ahmad, H. Nisar, S. Khan, R. Ullah, R. Rashid, H. Mahmood. Photodiagnosis and Photodynamic Therapy. 2016, 15, 94.

[33] M. Paraskevaidi, C. L. M. Morais, O. Raglan, K. M. G. Lima, E. Paraskevaidis, P. L. Martin-Hirsch, M. Kyrgiou, F. L. Martin. J Biophotonics. 2018, 11, e201700372.

[34] J. Prat. Int J Gynaecol Obstet. 2014, 124, 1.

[35] C. L. M. Morais, M. Paraskevaidi, L. Cui, N. J. Fullwood, M. Isabelle, K. M. G. Lima, P. L. Martin-Hirsch, H. Sreedhar, J. Trevisan, M. J. Walsh, D. Zhang, Y. G. Zhu, F. L. Martin. Nature Protocols. 2019, 14, 1546.

[36] R. Bro, A. K. Smilde. Analytical Methods. 2014, 6, 2812.

[37] C. L. M. Morais, K. M. G. Lima, M. Singh, F. L. Martin. Nature Protocols. 2020, 15, 2143.

[38] D. Ballabio, V. Consonni. Analytical Methods. 2013, 5, 3790.

[39] C. L. M. Morais, K. M. G. Lima. Journal of the Brazilian Chemical Society. 2018, 29, 472.

[40] C. Cortes, V. Vapnik. Machine Learning. 1995, 20, 273.

[41] D. B. Hibbert. IUPAC Recommendations 2016. 2016, 88, 407.

[42] R. G. Brereton, G. R. Lloyd. Journal of Chemometrics. 2014, 28, 213.

[43] C. L. M. Morais, M. C. D. Santos, K. M. G. Lima, F. L. Martin. Bioinformatics. 2019, 35, 5257.

[44] C. L. M. Morais, K. M. G. Lima. Chemometrics and Intelligent Laboratory Systems. 2017, 170, 1.

[45] S. Pahlow, K. Weber, J. Popp, B. R. Wood, K. Kochan, A. Ruther, D. Perez-Guaita, P. Heraud, N. Stone, A. Dudgeon, B. Gardner, R. Reddy, D. Mayerich, R. Bhargava. Appl Spectrosc. 2018, 72, 52.

[46] J. J. Wei, J. William, S. Bulun. Int J Gynecol Pathol. 2011, 30, 553.

[47] S. Böhm, A. Faruqi, I. Said, M. Lockley, E. Brockbank, A. Jeyarajah, A. Fitzpatrick, D. Ennis, T. Dowe, J. L. Santos, L. S. Cook, A. V. Tinker, N. D. Le, C. B. Gilks, N. Singh. J Clin Oncol. 2015, 33, 2457.

[48] L. Ashton, P. D. Pudney, E. W. Blanch, G. E. Yakubov. Advances in Colloid and Interface Science. 2013, 199-200, 66.

[49] H. S. Davies, P. Singh, T. Deckert-Gaudig, V. Deckert, K. Rousseau, C. E. Ridley, S. E. Dowd, A. J. Doig, P. D. Pudney, D. J. Thornton, E. W. Blanch. Analytical Chemistry. 2016, 88, 11609.

[50] G. Zhu, X. Zhu, Q. Fan, X. Wan. Spectrochim Acta A Mol Biomol Spectrosc. 2011, 78, 1187.

[51] A. Kirwan, M. Utratna, M. E. O'Dwyer, L. Joshi, M. Kilcoyne. Biomed Res Int. 2015, 2015, 490531.

[52] P. Giamougiannis, P. L. Martin-Hirsch, F. L. Martin. Carcinogenesis. 2021, 42, 327.

[53] J. Bian, B. Li, X. J. Kou, T. Z. Liu, L. Ming. Asian Pac J Cancer Prev. 2013, 14, 6241.

[54] Z. Movasaghi, S. Rehman, I. U. Rehman. Applied Spectroscopy Reviews. 2007, 42, 493.

[55] P. M. Willemse, R. W. van der Meer, J. Burggraaf, S. G. van Elderen, M. L. de Kam, A. de Roos, H. J. Lamb, S. Osanto Acta Oncol. 2014, 53, 351.

[56] W. Tian, Y. Yao, G. Fan, Y. Zhou, M. Wu, D. Xu, Y. Deng. PLoS One. 2019, 14, e0221866.

[57] G. Zhao, H. Cardenas, D. Matei. Cancers (Basel). 2019, 11.

[58] R. G. Moore, A. K. Brown, M. C. Miller, S. Skates, W. J. Allard, T. Verch, M. Steinhoff, G. Messerlian, P. DiSilvestro, C. O. Granai, R. C. Bast, Jr. Gynecol Oncol. 2008, 108, 402.

[59] S. K. Tay, E. K. Chua. Ann Acad Med Singap. 1994, 23, 311.

[60] M. V. Barbolina, N. M. Moss, S. D. Westfall, Y. Liu, R. J. Burkhalter, F. Marga, G. Forgacs, L. G. Hudson, M. S. Stack. Cancer Treat Res. 2009, 149, 319.

[61] C. R. Smith, I. Batruch, J. M. Bauça, H. Kosanam, J. Ridley, M. Q. Bernardini, F. Leung, E. P. Diamandis, V. Kulasingam. Clinical Proteomics. 2014, 11, 23.

[62] A. F. Chambers, B. C. Vanderhyden. Clin Cancer Res. 2006, 12, 323.

[63] A. Bertoluzza, C. Fagnano, P. Finelli, M. A. Morelli, R. Simoni, R. Tosi. Journal of Raman Spectroscopy. 1983, 14, 386.

[64] F. G. Lawton, M. Griffin, J. A. Slack, G. Blackledge. Br J Cancer. 1990, 62, 692.

[65] E. Ferrari, A. Wittig, F. Basilico, R. Rossi, A. De Palma, D. Di Silvestre, W. A. G. Sauerwein, P. L. Mauri. Molecules (Basel, Switzerland). 2019, 24.

[66] W. Jiang, T. Ma, C. Zhang, X. Tang, Q. Xu, X. Meng, T. Ma. Journal of Proteomics. 2020, 210, 103533.

[67] K. Grayson, E. Gregory, G. Khan, B. A. Guinn. Biomarkers in Cancer. 2019, 11, 1179299x19830977.

[68] H. Kim, H. K. Min, G. Kong, M. H. Moon. Anal Bioanal Chem. 2009, 393, 1649.

[69] S. Ferraro, F. Braga, M. Lanzoni, P. Boracchi, E. M. Biganzoli, M. Panteghini. J Clin Pathol. 2013, 66, 273.

[70] J. Lin, J. Qin, V. Sangvatanakul. Eur J Obstet Gynecol Reprod Biol. 2013, 167, 81.

[71] E. M. Meys, J. Kaijser, R. F. Kruitwagen, B. F. Slangen, B. Van Calster, B. Aertgeerts, J. Y. Verbakel, D. Timmerman, T. Van Gorp. Eur J Cancer. 2016, 58, 17.

[72] K. T. Zondervan, C. M. Becker, K. Koga, S. A. Missmer, R. N. Taylor, P. Viganò. Nat Rev Dis Primers. 2018, 4, 9.